A 9 GHz EPR Imager for Thin Materials: Application to Surface Detection

Kouichi Nakagawa[1]* , Yasunori Ohba[2], Boris Epel[3] and Hitoshi Hirata[4]

[1] Department of Radiological Life Sciences, Graduate School of Health Sciences, Hirosaki University (66-1 Hon-Cho, Hirosaki 036-8564, JAPAN)

[2] Institute of Multidisciplinary Research for Advanced Materials, Tohoku University (Katahira 2-1-1, Aoba-ku, Sendai 980-8577, JAPAN)

[3] Department of Radiation & Cellular Oncology, The University of Chicago (MC1105, 5841 S. Maryland Ave, Chicago, IL 60637-1463, USA)

[4] Division of Bioengineering and Bioinformatics, Graduate School of Information Science and Technology, Hokkaido University (North 14 West 9, Kita-ku, Sapporo 060-0814, JAPAN)

Abstract: A 9 GHz EPR imager that is capable of the imaging surface area of thin materials has been built. The EPR imager resolved samples spaced 1 mm apart. The developed TE_{111} cavity was able to detect easily ~1.0 mM aqueous TEMPOL solution in ~1.0 mm (i.d.) glass capillary placed just above the cavity. The sensitivity measured using the TEMPOL solution showed ~0.3 of that for the modified JEOL cavity, which was in a qualitative agreement with the calculations considering the difference in the filling factors of the cavities. The relatively low measured sensitivity of the TE_{111} cavity is due to utilization of the microwave field from ~3 mm aperture (hole) in the cavity wall. More importantly, the TE_{111} cavity does not require inserting the sample into the cavity and placing samples into EPR tubes.

Key words: EPR; imaging; free radical; DPPH; ESR cavity; skin; surface detection

1 INTRODUCTION

EPR（Electron Paramagnetic Resonance）or ESR（Electron Spin Resonance）spectroscopy utilizes the electron-spin resonance phenomenon, which measures the resonant absorption spectra of the unpaired electrons subjected to the constant magnetic field in an atom, a molecule, or a compound. When the overall motion of an unpaired electron in a material is changed, the resonance frequency of the individual electron is changed.

The principles behind magnetic resonance are common to both EPR and NMR（nuclear magnetic resonance）, but there are differences in the magnitudes and signs of the magnetic interactions involved. EPR probes an unpaired electron spin, while NMR probes a nuclear spin. Conventional EPR can easily detect a sample which contains 10^{12} spins and is more sensitive than NMR. Therefore, EPR techniques are able to elucidate structures as well as dynamics of thin materials such as skin lipid.

In the area of dermatological science, non-invasive spectroscopic characterization of the outermost layer of the stratum corneum（SC）is an important subject. The SC, a heterogeneous structure composed of corneocytes embedded in the intercellular lamellar lipid bilayer, acts as the main epidermal barrier against chemicals, oxidative stress, and the UV component of sunlight. However, no quantitative method is available to define the structures.

At present, EPR spin-probe method is available to define the structures and motions of the intercellular lamellar lipid bilayers of skin[1-4]. Transepidermal water loss （TEWL）measurement is the only non-invasive method that provides indirect knowledge regarding the status of the SC in relation to water permeation. The measurement of TEWL is the most popular method to estimate the state of the skin. The ordering of the SC lipid bilayer can be also studied by X-ray analysis only for *in vitro* SC specimens or model lipid membranes containing water[5]. However, these do not provide the clear structural information about the lipid in the SC.

The EPR spin-probe method has been applied to study skin lipid structure using a 9 GHz spectrometer[1-4]. Structural dependence as a function of skin depth was reported. In addition, sebum secretions were detected by the method. However, the applicability of EPR spectrometer used in these studies is limited due to necessity of the sample-tube insertion into the cavity space, which is typical for EPR measurements. The EPR imaging of the human skin was used previously to study free radical permeation and metabolism in human skin at 2.2 GHz[6]. The 9 GHz EPR imaging was performed to observe anthralin radical generation in mouse skin[7]. However, the 2.2 and 9

GHz imaging capabilities have not been fully investigated, yet.

In this report, we propose a new way of detecting unpaired electron spin on the surface of thin materials that does not require insertion of the sample-tube into an EPR resonator. A cylindrical cavity operating at a TE_{111} mode might be a favorable candidate for this application. TE mode stands for transverse electric mode. The microwave propagates along a guiding system with a longitudinal magnetic field and without longitudinal electric field components. The subscripts of TE_{mnp} are the number of half-wavelength patterns in the standing wave in three directions. To detect the EPR signal, we used the microwave field from a aperture in the resonator. Ikeya, et al. originally used the microwave field from a resonator aperture for EPR measurements that were difficult to locate at the center of the cavity[8].

We present the results of 9 GHz EPR imaging of a paramagnetic species spaced 1 mm apart and a new method of surface detection. The components of the 9 GHz imager and imaging data processing are discussed. The EPR imaging technique, which is described, could provide confirmatory information about surface structure and dynamic properties of the skin at a molecular level. In addition, we have developed a new TE_{111} cavity to detect a surface area. The calculation and estimation of the new resonator performance are also discussed.

2 EXPERIMENTAL

2.1 EPR cavity and cavity Q factor measurements

A commercially available JEOL RE-3X 9 GHz EPR spectrometer was modified for EPR imaging by the attachment of a magnetic-field gradient coil and its power supply. A commercial JEOL TE_{011} cavity（JEOL）and a newly developed TE_{111} cavity[9] were used for EPR measurements. The TE_{111} cavity with a sample aperture radius of 3 mm was fabricated in our laboratory from oxygen-free copper. Ikeya, et al. originally proposed the use of microwave field leakage for EPR measurements[8]. The quality factor（Q）of the cavities was measured using a Network Analyzer N5230A（Agilent Technologies, Santa Clara, CA）.

2.2 EPR measurements

For 9 GHz EPR imaging, a set of gradient coils with an anti-Helmholtz coil configuration was used. The gradient coils were cooled by water to avoid overheating. A Techron 7570 power supply（Indiana, USA）was used. The available maximum field gradient along the z-axis was approximately 9 mT/cm. Two paramagnetic species, DPPH（2,2-Diphenyl-1-picrylhydrazyl）and TEMPOL（4-hydroxy-2, 2, 6, 6-tretra-methylpiperidin-1-oxyl）, were purchased from Nacalai Tesque, Inc., and used as received. DPPH was solidified by

commercially available glue on a plastic rod（1 mm o.d.）. The phantom was inserted in the commercial JEOL TE_{011} cavity. The phantom was composed of 4 points of DPPH samples with the axes system, as shown in the inset of **Fig. 1**. The first and the second points were 1 mm apart. The third and the fourth points were 2 mm apart. The second and the third points were also 2 mm apart. Typical EPR spectrometer settings for the JEOL cavity were as follows:
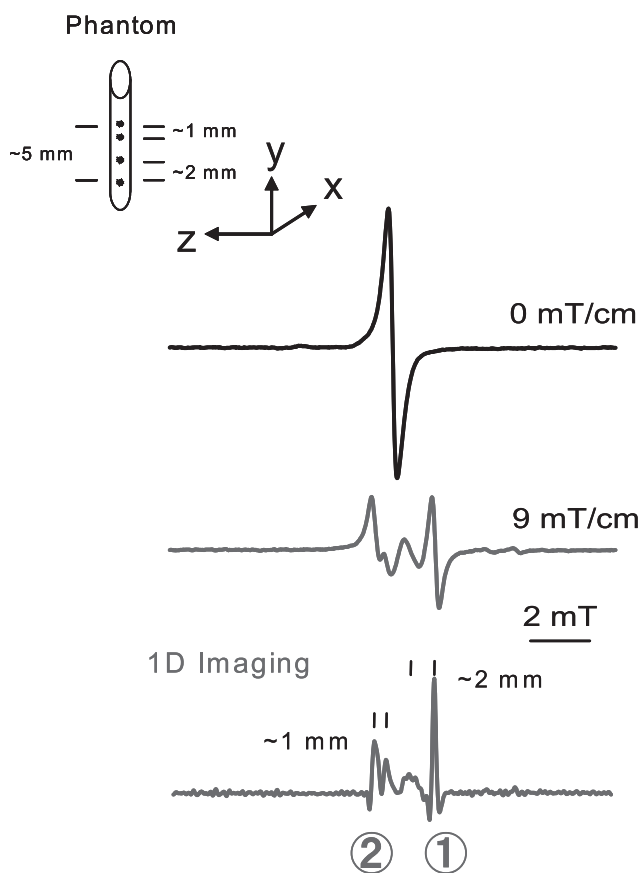

Fig. 1 One-dimensional EPR imaging of the phantom made by DPPH powder. The top trace is the first-derivative EPR absorption spectrum of the phantom without field gradient. The middle trace is the first-derivative EPR absorption spectrum under magnetic field gradient（9 mT/cm）, and the bottom trace is the spatial distribution of EPR signals. The modulation amplitude and frequency were 0.30 mT and 100 kHz, respectively. We chose higher modulation than the usual because of weakening the signal intensities under the field gradient. The field-swept derivative spectra were obtained by increasing the field gradient. The two strong peaks（① and ②）were indicated. The top-left hand inset is the phantom that is described in the text. The axes system of the imaging is also described.

microwave power, 5 mW; time constant, 1 s; sweep time, 2 min; magnetic field modulation, 0.3 mT; sweep width, 15 mT. All measurements were performed at ambient temperature.

2.3 Imaging data processing[10, 11]

All of the projections were preprocessed and deconvolved before the image reconstruction. The first-derivative EPR spectra were numerically integrated to obtain the corresponding absorption spectra. Approximations for the spectra at angles between $+90°$ and $-90°$ were obtained by extrapolation of the peak positions in the spectra obtained at the largest positive and negative gradients and convolution with Gaussian line-shapes.

For two-dimensional (2D) spectral-spatial EPR imaging, we used 25 projections obtained with gradients, G_i, from 0 to $\sim$9 mT/cm. The signals were integrated. The projections were centered on the crossover magnetic field, truncated to $SWEEP_i = \sqrt{2} dB/\cos(\Theta_i)$, where $\Theta_I = \tan^{-1}(G_i \times dL/dB)$, scaled by $\cos(\Theta_i)$ and resampled to 100 points. The magnetic field dimension, dB, was chosen to be 2 mT, and the spatial dimension, of the image was 1 cm. The projections with the negative gradients ($\Theta_i > \pi/2$) were obtained from the projections with $\Theta_i < \pi/2$. Then, the data were back-projected to obtain a 2D spectral-spatial image using a filtered back-projection algorithm. Data were processed in the Mathworks MATLAB™ environment, and the "iradon" function was used for back-projection.

3 RESULTS AND DISCUSSION

3.1 EPR imaging with JEOL TE$_{011}$ cavity

First, the maximum magnetic field gradient was established using the phantom with the DPPH points separated by 1 mm. Based on the peak distance in the EPR spectrum obtained with the maximum field gradient, the maximum gradient was estimated to be $\sim$9 mT/cm.

The top spectrum in **Fig. 1** shows the phantom measured without the field gradient. The schematic drawing of the phantom is shown in the inset of **Fig. 1**. The spectrum obtained is a single EPR line. The peak-to-peak line width is 0.258 mT. he line width is a little broader owing to the solidification of the DPPH with glue, the spatial distribution of DPPH powder, and the phantom rod alignment. The EPR intensity is maximum at the second position from the bottom of the phantom in the cavity. However, we measured the phantom from a position near the middle of the phantom.

The middle spectrum in **Fig. 1** shows the phantom measured with the maximum field gradient. The four overlapped EPR lines are clearly separated. The bottom spectrum in **Fig. 1** shows the spatial distribution of EPR signals, i.e., unpaired electron spins in the phantom. The spatial

profile of the bottom spectrum was obtained by a process of deconvolution between the above two traces. Again, the four peaks are very clear. Thus, the EPR imager is able to resolve objects of the paramagnetic species separated by at least 1 mm.

Fig. 2 shows a 2D (spectral-spatial) image of the phantoms. The range of color map intensities was chosen to show the weaker signals. The maximum of the strongest peak was thus clipped at approximately half intensity. The two areas indicated by ① and ② correspond to the two strong peaks of the 1D spectrum in **Fig. 1**. The weaker point was missed during the data processing. Thus, it is necessary to improve the data processing in order to reflect the EPR data in the imaging.

Fig. 3 shows the reconstructed spectra for the 2D EPR imaging as a function of the magnetic field and the spatial distribution. The top part of **Fig. 3** shows the spatial dimension at the maximum of EPR lines. After the data processing, three strong peaks were obtained. The bottom part of Fig. 3 shows the EPR absorption (integrated derivative) signal as a function of the magnetic field. Two EPR spectra at spatial positions ① and ② are displayed.

3.2 Comparison and calculation of modified JEOL TE$_{011}$ and newly developed TE$_{111}$ cavity

A new TE$_{111}$ cavity for measuring signals from the surface of thin materials was developed[9]. The cavity is different from the conventional cavity in its design of field
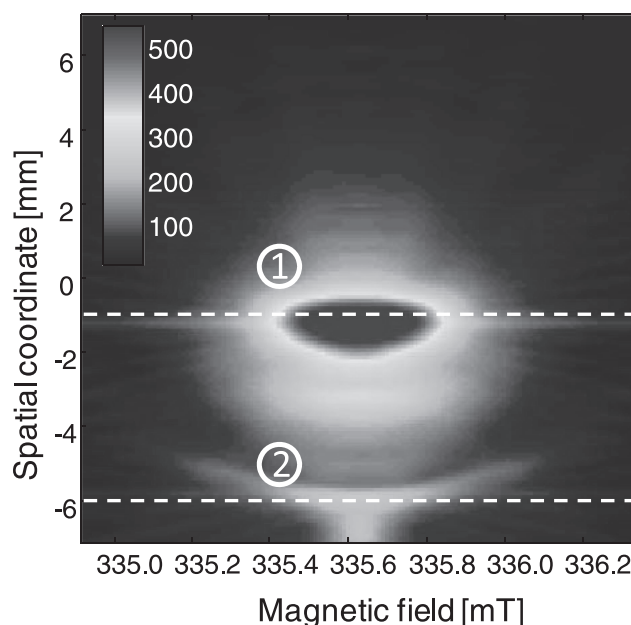

Fig. 2 The two dimensional (2D) (spectral-spatial) imaging of the phantom is shown. The axes system of the imaging is also described. The two strong peaks (① and ②) are related to the strong EPR signals of the 1D imaging in Fig. 1.
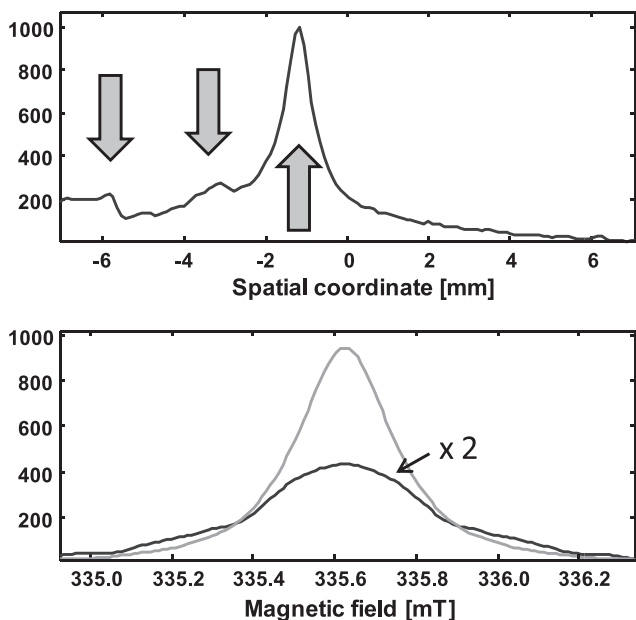
Fig. 3 Two compositional diagrams of the 2D imaging in Fig. 2 are presented. The top and bottom spectra refer to the position in the y-direction and the magnetic field direction in Fig.2, respectively. The arrows indicate three strong signals of the phantom. The bottom spectra are the absorption（integrated derivative）EPR spectra. The ① and ② indicate the distinguishable phantom signals.

Fig. 4 Schematic drawing of a newly developed surface-detection method for EPR imaging spectroscopy is presented. The field modulation coils are placed above the TE_{011} cavity.

Fig. 5 Cavity configurations of a）cylindrical TE_{111}, the inner diameter $a = 14$ mm, the length $L = 21$ mm and b）cylindrical TE_{011}, $a = 21$ mm, $L = 42$ mm. S is the sample hole, circular or rectangular; C is the microwave coupling hole; r and ϕ are defined in a plane perpendicular to z. The H and E represent the magnetic and electric flux, respectively.

modulation coils and the sample position, as depicted in Fig. 4. Fig. 4 illustrates the new method of placing sample material on top of the cavity instead of inserting it into the cavity（the most common usage）. It is noted that the location of field modulation coils outside of the cavity is very different from that of the commercial TE_{011} cavity. Therefore, it is possible to measure and image thin materials such as skin surfaces instead of measuring signal from the whole sample.

To observe EPR of a sample outside the cavity, a small aperture from which the microwave field leaks was designed in the cavity wall. The aperture location was chosen to provide maximum leakage of the microwave magnetic field and minimum leakage of the electric field as shown in Fig. 5. We compared the sensitivities of a cylindrical cavity resonator TE_{111} and a modified JEOL TE_{011}. The commercially available JEOL TE_{011} cavity has an aperture in its front for light irradiation of a sample. We modified the cavity by attaching field modulation coils in the same manner as the TE_{111} cavity and used the aperture for the measurements removing a choke structure that prevents microwave leakage.

A high-intensity microwave magnetic field is important to obtain higher sensitivity. However, a high-intensity microwave electric field leads to degradation of Q. An exact
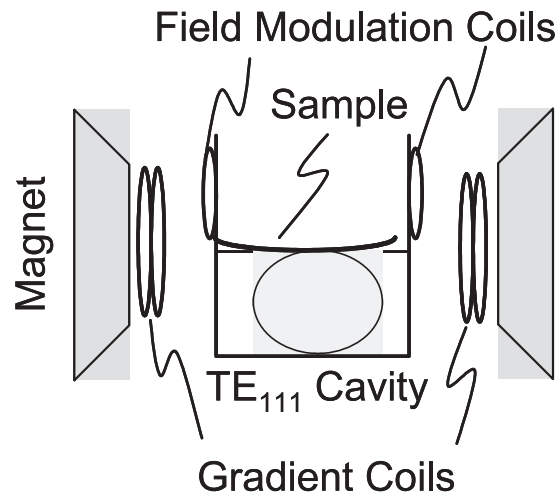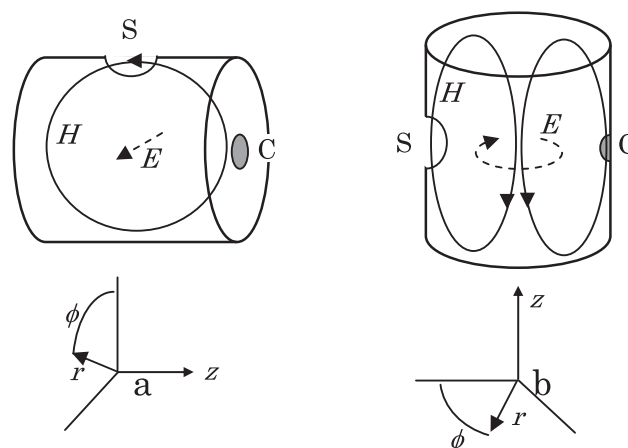
theoretical analysis of the sensitivity of the new design is complicated because this cavity configuration is not conventional. Here, we apply simple theoretical considerations. In general, the sensitivity of a cavity is proportional to the product of the filling factor and cavity $Q^{12)}$. We used the following analytical expression to calculate the Q values, neglecting the effects of the sample and the coupling holes[12].

For a cylindrical cavity operating in a TE_{mnp} mode, the Q and the z component of magnetic field H are expressed by:

$$Q\frac{\delta}{\lambda}=\frac{(1/2\pi)\left[1-m/\rho'^2_{mn}\right]\left[\rho'^2_{mn}+(p\pi a/L)^2\right]^{3/2}}{\rho'^2_{mn}+(2a/L)(p\pi a/L)^2+(1-2a/L)\left[mp\pi a/L\rho'_{mn}\right]^2}$$

$$(1)$$

$$\frac{1}{\lambda}=\frac{1}{2a}\left[\left(\frac{(k_c a)'_{mn}}{\pi}\right)^2+\left(\frac{pa}{L}\right)^2\right]^{1/2}$$

where m, n, and p are the number of half-wavelength patterns in the standing wave in ϕ, r, and z directions, respectively, as defined in **Fig. 5**. The δ is the skin depth of cavity's inner walls, λ is the wavelength of the microwave, a is the inner diameter, L the cavity length in z, and ρ'_{mn} is the nth root of the first derivative of the mth order Bessel function of the first kind, $J_m(x)$. In Eq. (1), an error is corrected[12].

The results of the theoretical sensitivity were examined by estimations of the quality factors of the cavities[8, 12]. **Fig. 6** shows the frequency-response curve as a function of the microwave frequency.

The filling factor is a measure of the efficiency of the microwave irradiation and is defined by:

$$\eta=\frac{\int_{Sample}|H_z|^2 dV}{\int_{Cavity}|\mathbf{H}|^2 dV}$$

$$(2)$$

where $\mathbf{H}$ is the microwave magnetic field vector. H_z represents the z component of $\mathbf{H}$ inside the sample, which is perpendicular to the external static magnetic field and causes EPR transitions. H_z at a position (r,ϕ,z) is given by:

$$H_z(r,\phi,z)=H_{mnp}J_m(\rho'_{mn}r/a)\cos m\phi\sin\left(\frac{p\pi z}{L}\right)$$

$$(3)$$

where H_{mnp} is a constant determined by the input microwave energy. We calculated η under the following assumptions: (a) $H_z(r,\phi,z)$ at the outside of the sample aperture is proportional to H_z on the wall, $H_z(a,\phi,z)$. (b) The ratio

between $H_z(r,\phi,\sim0)$ and $H_z(0,\phi,z)$ is the same for the two modes. (c) The decay of H_z outside the cavity along the radial direction is negligible inside the sample; the sample thickness is much less than the 9 GHz microwave wavelength (about 30 mm), and the field leakage decays exponentially with a characteristic distance approximately equal to λ. (d) The product of the denominator in Eq. (2) and the permeability, μ, is the same as the energy stored in the unperturbed cavity, W_c:

$$W_c=\mu\mid H_{mnp}\mid^2\frac{\pi^3 L a^4}{\lambda^2\rho'^4_{mn}}\left(\rho'^2_{mn}-m^2\right)J_m^2(\rho'_{mn})$$

Assuming constant H_z over the sample thickness, we approximated the filling factor as,

$$\eta=\frac{d_s}{W_c/\mu}\int_{HolePlane}\mid H_z\mid^2 dS$$

$$(4)$$

where d_s the thickness of the sample. The surface area element on the cavity wall is indicated by ds. Eq. (4) is integrated numerically.

3.5 Measurements of spin probe TEMPOL

The sensitivity of the new TE$_{111}$ cavity was estimated using $\sim$1.0 mM aqueous TEMPOL solution in a $\sim$1.0 mm (i.d.) glass capillary. **Fig. 7** shows EPR spectra of TEMPOL obtained by the TE$_{111}$ and modified TE$_{011}$ cavities. The sensitivity of the new cavity is approximately 0.3 of the JEOL TE$_{011}$ cavity sensitivity. The relatively weak sensitivity of the surface detection is mainly due to the use of relatively weak microwaves leakage from the small aperture ($\sim$3 mm diameter) in the cavity to detect the sample. It is notable that the surface measurements do not require placing the samples into the inner volume of the cavity as well as placing samples into EPR tubes. The measurements using the TE$_{111}$ cavity can be performed using high-power microwaves to compensate for the weak signal intensity.
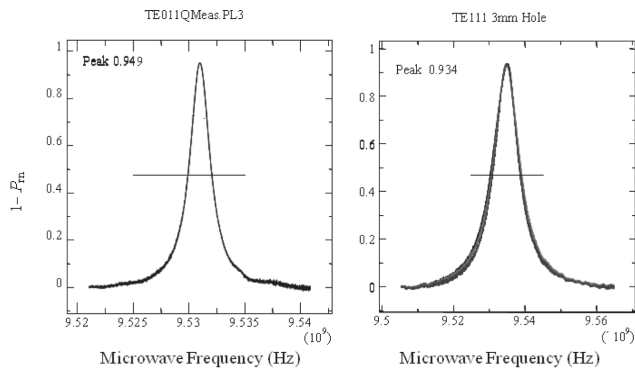

Fig. 6 Plot of the frequency-response curve as a function of the microwave frequency. The frequency-response curves of TE$_{011}$ (left-hand side) and TE$_{111}$ (right-hand side) were presented. The P_m is the normalized power, which is the reflected power from the cavity divided by input power. The lines represent the half-power points on the response curves.

Table 1 Parameters of the relative sensitivity for the cavities.

	TE$_{011}$ (Cyl.)	TE$_{111}$ (Cyl.)
a (mm)	21	14
d (mm) or L	42	21
f (GHz)	9.40	9.50
Q	15000	6500
$\eta/d_s\lambda^2$ (m^{-3})	4.1×10^{2} [a]	1.4×10^{3} [a]
$\eta Q/d_s\lambda^2$ (m^{-3})	1.28×10^{7} [a]	1.75×10^{7} [a]
TEMPOL ($\sim$1.1 mM) detection	1	$\sim$0.33

Notes: TE$_{011}$ (Cyl.) is the JEOL modified cavity; TE$_{111}$ (Cyl.) is the new cavity developed.

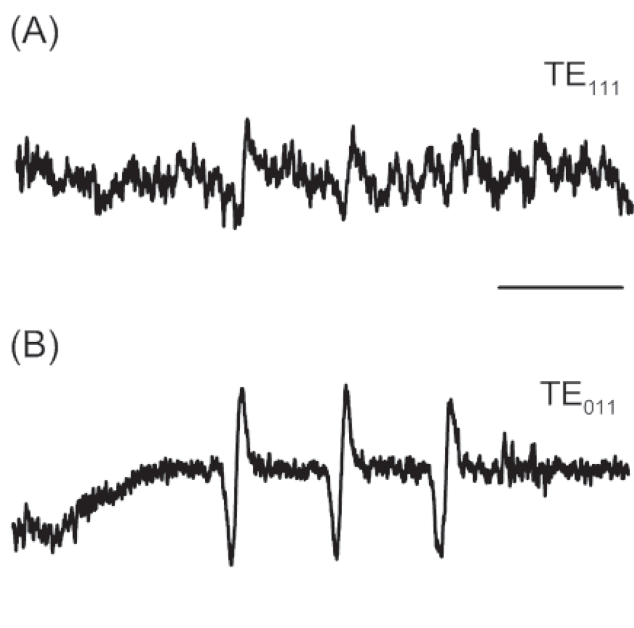a) is the sample aperture of 3 mm diameter for TE$_{111}$.

455

Fig. 7. Experimental spectra of TEMPOL were obtained by TE_{111} (A) and TE_{011} (B) cavities, respectively. The EPR settings for both measurements were as follows: microwave power, 10 mW; time constant, 0.1 s; sweep time, 2 min; magnetic field modulation, 0.2 mT; sweep width, 10 mT. However, the TE_{111} and TE_{011} cavities were connected to waveguide and coaxial cable, respectively. The Y-axis ranges from -600 to $+600$ for both spectra. The bars indicate 2 mT.

4 CONCLUSIONS

The 9 GHz EPR imager was constructed to detect the surface area of thin materials The 1D EPR imaging was able to resolve samples separated by 1 to 2 mm. The new spectrometer was also capable of the 2D (spectral-spatial) imaging. The EPR imager is able to measure various thin films and materials. In addition, we applied a new surface detection method. The newly designed TE111 cavity is able to detect ~1.0 mM TEMPOL solution. The new surface method does not require placing the sample into the cavity. A particularly plausible application of the new design is to measure skin surfaces to reveal permeation of various spin probes in the stratum corneum.

REFERENCES

1) Nakagawa, K. Elucidated Lipid Structures of Various Human Stratum Corneum Investigated by EPR Spectroscopy. *Skin Res. Technol.* **17**, 245-250 (2011).

2) Nakagawa, K; Anzai, K. Stratum Corneum Lipid Structure Investigated by EPR Spin-Probe Method: Application of Terpenes. *Lipids.* **45**, 1081-1087 (2010).

3) Nakagawa, K. Electron Paramagnetic Resonance Investigation of Stratum Corneum Lipid Structure. *Lipids.* **45**, 91-96 (2010).

4) Nakagawa, K; Anzai, K. Stratum Corneum Lipid of Hairless Mouse Investigated by Electron Paramagnetic Resonance. *Appl. Magn. Reson.* **40**, 557-565 (2011).

5) Pilgram, G. S. K.; Engelsma-Van Pelt, A. M.; Bouwstra, J. A.; Koerten, H. K. Electron diffraction provides new information on human stratum corneum lipid organization studied in relation to depth and temperature. *J. Invest. Dermatol.* **113**, 403-409 (1999).

6) He, G.; Samouilov, A.; Kuppusamy, P.; Zweier, J.L. In vivo EPR imaging of the distribution and metabolism of nitroxide radicals in human skin. *J Magn. Reson.* **148**, 155-160 (2000).

7) Matsumoto, K.; Kawai, S.; Chignell, C. F.; Utsumi, H. Location of anthralin radical generation in mouse skin by UV-A irradiation: an estimation using microscopic EPR spectral-spatial imaging. *Magn. Reson. Med.* **55**, 738-742 (2006).

8) Hochi, A.; Furusawa, M.; Ikeya, M. Applications of Microwave Scanning ESR Microscope: Human Tooth with Metal, Appl. Rad. Isotopes, 401-405 (1993).

9) Nakagawa, K. Jpn. Pat., 2010-163278, submitted (2010).

10) Maltempo, M. M. Differentiation of Spectral and Spatial Components in EPR Imaging Using 2-D Image Reconstruction Algorithms, *J. Magn. Reson.* **69**, 156-161 (1986).

11) Maltempo, M. M.; Eaton, S. S.; Eaton, G. R. Spectral-Spatial Two-Dimensional EPR Imaging, *J. Magn. Reson.* **72**, 449-455 (1987).

12) Charles P. Poole, Jr., Electron spin resonance 2nd ed., Chapter 5, Section D. Cylindrical Resonant Cavities on page 135 and Section H. Filling Factors on page 156, John Wiley & Sons, Inc., New York (1983).

13) Ohba, Y.; Watanabe, C.; Nakazawa, S.; Yamauchi, S. Determination of Quality Factor for Highly Overcoupled EPR Resonators, *Appl. Magn. Reson.* **37**, 781-794 (2010).